ELECTRO-MAGNETOHYDRODYNAMIC PERISTALTIC PUMPING OF A BIVISCOSITY FLUID BETWEEN TWO COAXIAL DEFORMABLE TUBES THROUGH A POROUS MEDIUM

H. Rachid[†], M.T. Ouazzani

Department of Physics, Faculty of Sciences Ain Chock
University Hassan II, Maarif, Casablanca, Morocco

(Received August 2, 2017; accepted September 26, 2017)

This article aims at analyzing the electro-magnetohydrodynamic (EMHD) flow of a biviscosity fluid in a peristaltic endoscope and through a porous medium. Both the inner and outer tubes have sinusoidal wave traveling down their walls where there is a coupling between the occlusion of the outer tube and the radius ratio. The analytical solutions are found under long wavelength and low Reynolds number assumptions. The influences of the electrical field strength parameter H, Hartmann number M, upper limit apparent viscosity coefficient β, Darcy number Da, occlusion ϕ and the radius ratio n on the axial velocity w, pressure gradient $\frac{\partial p}{\partial z}$, pressure rise Δp, and on mechanical efficiency E are discussed through graphs. The results show that E increases with increasing all parameters except the Hartmann number. Moreover, the peristaltic pumping regions, the pressure rise for zero flow rate, and the flow rate in the absence of a pressure rise are graphically discussed.

DOI:10.5506/APhysPolB.48.1515

1. Introduction

Peristaltic pumping or peristalsis is a fundamental biomechanical mechanism when the fluid is transported by a progressive wave of contraction and expansion of the muscles which pumps this fluid. This phenomenon is used in the physiological vessels such as oesophagus, stomach, intestines, sometimes in the ureters, and blood vessels (arteries, veins, capillaries *etc.*). Due to the importance of peristalsis, it has become the object of scientific research, since the first investigation of peristaltic transport for a Newtonian fluid by Latham [1]. For non-Newtonian fluids and in different geometries, several researchers have attempted to analyze this type of flows. For example, Fung and Yih [3] have studied the peristaltic pumping of a viscous fluid

[†] Corresponding author: `rhassan2@yahoo.fr`

in a channel. Srivastava *et al.* [4] have analyzed the peristaltic transport of a physiological fluid of variable viscosity in a non-uniform tube and channel. Abbasi *et al.* [5] have studied the peristaltic transport of an aqueous solution of silver nanoparticles with convective heat transfer at the boundaries. Shahzadi and Nadeem [6] have analyzed the impact of curvature on the mixed convective peristaltic flow of shear thinning fluid with nanoparticles. Hayat *et al.* [7] have investigated the peristaltic mechanism of a compressible Jeffrey fluid in a circular tube. The interaction of peristaltic transport with the pulsatile flow of a Maxwell fluid in a tube has been analyzed by Rachid and Ouazzani [8]. Recently, the effect of an inserted endoscope on peristaltic pumping has been studied in several articles. Akbar and Nadeem have analyzed the peristaltic flow of a Jeffrey fluid or of a nanofluid in an endoscope, respectively [9, 10]. The peristaltic transport of a Newtonian fluid through a uniform and non-uniform annulus has been presented by Mekheimer [11]. El Misery *et al.* [12] have examined the effects of an endoscope and variable viscosity on peristaltic motion. Rachid *et al.* [13] have analyzed the interaction of pulsatile flow and peristaltic transport of a Newtonian fluid in an endoscope. In all these studies, the endoscope is supposed rigid and uniform. For a deformable endoscope, Rachid and Ouazzani [14] have examined the peristaltic flow of a Newtonian fluid when the phases and the mean radius of the tubes are different.

Microfluidics plays an essential role in science and technology of manipulating and controlling fluids. It is very attractive for both academic researchers and industrials because of the wide range of applications such as electroosmosis micropumps [15–17], electrohydrodynamic micropumps [18–20] and electro-magnetohydrodynamic (EMHD) micropumps [21–23]. Recently, some researchers have studied the effect of a magnetic field (MHD) on peristaltic transport. For example, Eldesoky [24] has investigated the influence of slip conditions, body acceleration and a magnetic field on unsteady peristaltic flow through a porous medium in an artery. The MHD peristaltic transport of the Eyring–Powell fluid with heat/mass transfer, wall properties and slip conditions has been studied by Hina [25]. Hayat and Hina [26] have studied the influence of wall properties on the MHD peristaltic flow of a Maxwell fluid with heat and mass transfer. Another investigations dealing with the impact of magnetic field on peristaltic pumping are cited in Refs. [27–30]. In all these investigations, the electric field has not been taken into account. In this paper, we analyze the influences of a magnetic and an electric fields of a biviscosity fluid in a peristaltic endoscope through a porous medium. We suppose that the occlusion of the outer tube is coupled with the mean radius of the endoscope. The impact of physical parameters on pumping characteristics are discussed through graphs.

2. Formulation and analysis

Let us consider the EMHD flow of an incompressible and electrically conducting biviscosity fluid with density ρ and electrical conductivity σ through the gap between two coaxial peristaltic tubes. Both the inner and the outer tubes have sinusoidal waves traveling down their walls (*cf.* Fig. 1).

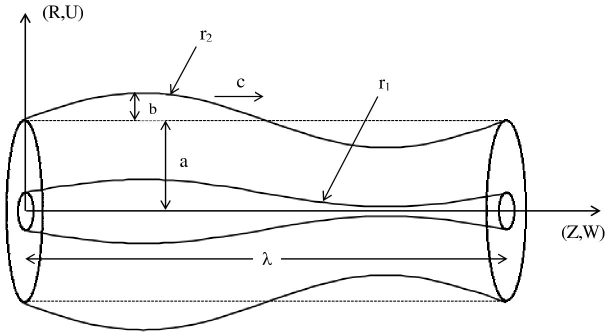

Fig. 1. Geometry of the problem.

In the fixed frame $(\bar{R}, \theta, \bar{Z})$, the geometry of the walls surfaces are described as

$$\begin{aligned} \bar{R}_2 &= a + b \, \sin \frac{2\pi}{\lambda} \left(\bar{Z} - c\bar{t} \right) , \\ \bar{R}_1 &= n \, \bar{R}_2 = na + nb \sin \frac{2\pi}{\lambda} \left(\bar{Z} - c\bar{t} \right) , \qquad 0 < n < 1 , \end{aligned} \tag{1}$$

where a is the radius of the outer tube at inlet, b is the wave amplitude, λ is the wavelength, c is the propagation velocity, $\bar{t}$ is the time.

The flow is driven by the Lorenz force, $\vec{J} \times \vec{B}$ in the e_z-direction generated by the interaction between the magnetic field $\vec{B}(0, B_0, 0)$ and the electric field $\vec{E}(E_0, 0, 0)$, where $\vec{J} = \sigma(\vec{E} + \vec{\bar{V}} \times \vec{B})$ denotes current density and $\vec{\bar{V}}(\bar{U}, \bar{V}, \bar{W})$ is the vector velocity in the fixed frame.

The constitutive equations for incompressible biviscosity fluids [31, 32] are defined as follows:

$$\tau = \begin{cases} 2 \left(\mu_\beta + p_y / \sqrt{2\pi} \right) e_{ij} \, , & \pi \geq \pi_c \, , \\ 2 \left(\mu_\beta + p_y / \sqrt{2\pi_c} \right) e_{ij} \, , & \pi < \pi_c \, , \end{cases} \tag{2}$$

where μ_β is the plastic viscosity of the fluid, p_y is yield stress and $\pi = e_{ij}$, e_{ij} is the (i, j) is the component of deformation rate with

$$e_{ij} = \frac{1}{2} \left(\frac{\partial v_i}{\partial x_j} + \frac{\partial v_j}{\partial x_i} \right) . \tag{3}$$

We introduce the following non-dimensional parameter $\beta = \mu_\beta\sqrt{2\pi_c}/p_y$ which denotes the upper limit apparent viscosity coefficient. For the ordinary Newtonian fluid, $p_y = 0$.

In the fixed frame $(\bar{R}, \bar{Z})$, the flow is unsteady but if we choose moving coordinates $(\bar{r}, \bar{z})$, then the flow can be treated as steady. The coordinates frames are related through

$$\bar{r} = \bar{R}; \qquad \bar{z} = \bar{Z} - c\bar{t}; \qquad \bar{p} = \bar{P}; \tag{4}$$

$$\bar{u}(\bar{r}, \bar{z}) = \bar{U}\left(\bar{R}, \bar{Z} - c\bar{t}\right); \qquad \bar{w}\left(\bar{r}, \bar{z}\right) = \bar{W}\left(\bar{R}, \bar{Z} - c\bar{t}\right) - c, \tag{5}$$

where $(\bar{u}, \bar{w})$ are the radial and axial components of velocity in the wave frame.

Taking into account the magnetic Lorentz force, the equations governing the EMHD fluid flow in the wave frame are:

$$\begin{aligned}
\frac{\partial \bar{u}}{\partial \bar{r}} + \frac{\bar{u}}{\bar{r}} + \frac{\partial \bar{w}}{\partial \bar{z}} &= 0, && (6)\\
\rho\left[\bar{u}\frac{\partial \bar{u}}{\partial \bar{r}} + \bar{w}\frac{\partial \bar{u}}{\partial \bar{z}}\right] &= -\frac{\partial \bar{p}}{\partial \bar{r}} + \frac{1}{\bar{r}}\frac{\partial}{\partial \bar{r}}\left(\bar{r}\bar{S}_{\bar{r}\bar{r}}\right) + \frac{\partial \bar{S}_{\bar{r}\bar{z}}}{\partial \bar{z}} - \frac{\mu}{k_0}\bar{u}, && (7)\\
\rho\left[\bar{u}\frac{\partial \bar{w}}{\partial \bar{r}} + \bar{w}\frac{\partial \bar{w}}{\partial \bar{z}}\right] &= -\frac{\partial \bar{p}}{\partial \bar{z}} + \frac{1}{\bar{r}}\frac{\partial}{\partial \bar{r}}\left(\bar{r}\bar{S}_{\bar{r}\bar{z}}\right) + \frac{\partial \bar{S}_{\bar{z}\bar{z}}}{\partial \bar{z}}\\
&\quad + \sigma E_0 B_0 - \left(\sigma B_0^2 + \frac{\mu}{k_0}\right)(\bar{w} + 1), && (8)
\end{aligned}$$

where $\bar{S}$ is the extra stress tensor, $\bar{p}$ is the pressure and k_0 is the permeability of the porous medium.

Here, we use the following dimensionless quantities:

$$\begin{aligned}
z &= \frac{\bar{z}}{\lambda}; \quad r = \frac{\bar{r}}{a}; \quad t = \frac{c\bar{t}}{\lambda}; \quad u = \frac{\lambda\bar{u}}{ac}; \quad w = \frac{\bar{w}}{c}; \quad p = \frac{a^2\bar{p}}{\mu_\beta\lambda c};\\
Q &= \frac{\bar{Q}}{\pi c a^2}; \quad q = \frac{\bar{q}}{\pi c a^2}; \quad S = \frac{a\bar{S}}{\mu_\beta c}; \quad \phi = \frac{b}{a}; \quad \delta = \frac{a}{\lambda};\\
\mathrm{Da} &= \frac{k_0}{a^2}; \quad \mathrm{Re} = \frac{\rho a c}{\mu_\beta}; \quad M = aB_0\left(\frac{\sigma}{\mu}\right)^{1/2}; \quad H = \frac{aE_0}{c}\left(\frac{\sigma}{\mu}\right)^{1/2}, \qquad (9)
\end{aligned}$$

where Q and q are the flow rates in the fixed and in the wave frames, respectively. δ is the dimensionless wave number, Re is the Reynolds number, Da is the Darcy number, M is the Hartmann number, H is the electrical field strength parameter, ϕ is the amplitude ratio with $0 < \phi < 1$.

Using the above non-dimensional quantities and under the assumptions of long wavelength approximation (*i.e.*, $\delta \ll 1$ or $\lambda \gg a$) and low Reynolds number (*i.e.*, $\mathrm{Re} \to 0$), the continuity equation is satisfied, and the equations of motion (6)–(8) can be reduced to

$$\begin{cases} \dfrac{\partial p}{\partial r} = 0\,, \\ \dfrac{1}{r}\dfrac{\partial}{\partial r}\left(r\dfrac{\partial w}{\partial r}\right) - N^2(w+1) = \alpha\dfrac{\partial p}{\partial z} - \alpha H M\,, \\ \dfrac{\partial u}{\partial r} + \dfrac{u}{r} + \dfrac{\partial w}{\partial z} = 0\,; \end{cases} \tag{10}$$

here, $\alpha = \dfrac{1}{(1+\frac{1}{\beta})}$ and $N^2 = \alpha\left(M^2 + \dfrac{1}{\mathrm{Da}}\right)$.

The boundary conditions which describe the velocity are

$$\begin{cases} w = -1 \quad \text{at} \quad r = r_1 = n + n\phi\sin(2\pi z)\,, \\ w = -1 \quad \text{at} \quad r = r_2 = 1 + \phi\sin(2\pi z)\,. \end{cases} \tag{11}$$

From the expression of r_1, it appears clearly that there is a coupling between the occlusion of the outer tube ϕ and the radius ratio $n = \dfrac{r_1}{r_2}$.

Integrating (10) and using the boundary conditions (11), we obtain the following solution:

$$w(r,z) = -1 + \frac{\alpha\left[\frac{\partial p}{\partial z} - MH\right]}{N^2}\Big(A_1 I_0(Nr) + A_2 K_0(Nr) - 1\Big) \tag{12}$$

with

$$\begin{aligned} A_1 &= \frac{K_0(Nr_2) - K_0(Nr_1)}{I_0(Nr_1)K_0(Nr_2) - I_0(Nr_2)K_0(Nr_1)}\,, \\ A_2 &= \frac{I_0(Nr_1) - I_0(Nr_2)}{I_0(Nr_1)K_0(Nr_2) - I_0(Nr_2)K_0(Nr_1)}\,, \end{aligned} \tag{13}$$

where I_0 is the modified Bessel function of the first kind of the order of 0, K_0 is the modified Bessel function of the second kind of the order of 0.

The instantaneous volume rate of flow in the fixed frame is given by

$$Q(Z,t) = 2\int\limits_{r_1}^{r_2} WR\,\mathrm{d}R = q + \left(r_2^2 - r_1^2\right) = q + \left(1 - n^2\right) r_2^2\,. \tag{14}$$

We calculate the time-averaged flow rate as follows:

$$Q = \int_0^1 Q(Z,t)\ \mathrm{d}t = q + \left(1 - n^2\right)\left(1 + \frac{\phi^2}{2}\right), \tag{15}$$

where q is the volume rate of flow in the wave frame, and it is given by

$$q = 2\int_{r_1}^{r_2} wr\ \mathrm{d}r\,. \tag{16}$$

Introducing velocity (12) into (16), we find

$$q = \frac{\alpha A_6}{N^3}\left[\frac{\partial p}{\partial z} - MH\right] - \left(r_2^2 - r_1^2\right) = \frac{\alpha A_6}{N^3}\left[\frac{\partial p}{\partial z} - MH\right] - \left(1 - n^2\right) r_2^2 \tag{17}$$

with

$$\begin{aligned} A_3 &= r_2 I_1(Nr_2) - r_1 I_1(Nr_1)\,; & A_4 &= r_1 K_1(Nr_1) - r_2 K_1(Nr_2)\,; \\ A_5 &= r_1^2 - r_2^2\,; & A_6 &= 2A_1A_3 + 2A_2A_4 + NA_5\,. \end{aligned} \tag{18}$$

Using (14) and (15), from Eq. (17), we find the pressure gradient as follows:

$$\frac{\mathrm{d}p}{\mathrm{d}z} = \frac{N^3\left[Q + \left(1 - n^2\right)\left(r_2^2 - 1 - \frac{\phi^2}{2}\right)\right]}{\alpha A_6} + MH\,. \tag{19}$$

The pressure rise Δp across one wavelength, in its non-dimensional form, is given by

$$\Delta p = \int_0^1 \frac{\partial p}{\partial z}\ \mathrm{d}z\,. \tag{20}$$

Introducing (19) into (20), we obtain the following expression of the pressure rise:

$$\Delta p = \frac{N^3}{\alpha}\int_0^1 \frac{Q + \left(1 - n^2\right)\left(r_2^2 - 1 - \frac{\phi^2}{2}\right)}{A_6}\ \mathrm{d}z + HM\,. \tag{21}$$

The mechanical efficiency is defined as the ratio between the average rate per wavelength at which work is done by the moving fluid against a pressure head and the average rate at which the walls do work on the fluid [33]. We obtain the expression of the mechanical efficiency as follows [34]:

$$E = \frac{Q\Delta p}{\left[\Delta p\left(r_2 - r_1\right)^2_{(z=0)} + F^{(\mathrm{i})} + F^{(\mathrm{o})} + 2I\right]}, \tag{22}$$

where $F^{(\mathrm{o})}$ and $F^{(\mathrm{i})}$ are the frictional forces on outer and inner tubes across one wavelength, respectively. They are given by

$$F^{(\mathrm{o})} = \int_0^1 -r_2^2 \frac{\partial p}{\mathrm{d}z}\,\mathrm{d}z\,, \tag{23}$$

$$F^{(\mathrm{i})} = \int_0^1 -r_1^2 \frac{\partial p}{\mathrm{d}z}\,\mathrm{d}z = n^2 \int_0^1 -r_2^2 \frac{\partial p}{\mathrm{d}z}\,\mathrm{d}z = n^2 F^{(\mathrm{o})} \tag{24}$$

and

$$I = \int_0^1 r_1 r_2 \frac{\partial p}{\partial z}\,\mathrm{d}z = n \int_0^1 r_2^2 \frac{\partial p}{\partial z}\,\mathrm{d}z = -nF^{(\mathrm{o})}\,. \tag{25}$$

Then the mechanical efficiency becomes

$$E = \frac{Q\Delta p}{\left[\Delta p\left((1-n)r_2\right)^2_{(z=0)} + (n-1)^2 F^{(\mathrm{o})}\right]}\,. \tag{26}$$

3. Results and discussions

The graphical results of the peristaltic characteristics *versus* different embedded parameters and the physical interpretation of these results are presented in this section. Before, we note that when $\beta \to \infty$, $\mathrm{Da} \to \infty$, $H = 0$, $M = 0$ and $n = 0$, we find the results of Shapiro *et al.* [33]. Figures 2 (a)–(f) display the variations of the axial velocity w with respect to the radial r. These figures show that w increases with increasing the electrical field strength parameter H, Hartmann number M, upper limit apparent viscosity coefficient β, Darcy number Da, occlusion ϕ, while it decreases with the increase in the radius ratio n.

The pressure gradient $\frac{\partial p}{\partial z}$ has been plotted in Figs. 3 (a)–(f). First, these figures show that $\frac{\partial p}{\partial z}$ is small in the large gap between the two tubes, whereas it is big in the narrow part. Figures 3 (c), (d) show that Da and β reduce the pressure gradient. From Figs. 3 (a), (b), (e), one can observe that an increase in H, M and n enhance the pressure gradient. It can be analyze from Fig. 3 (f) that the occlusion increases the pressure gradient in the narrow region, while we observe the opposite behavior in the large region.

The influences of the physical parameters on pressure rise Δp *versus* the time-averaged flow rate Q are presented in Figs. 4 (a)–(f). From Figs. 4 (a), (b), it can be seen that for different values of E and ϕ, respectively, the curves

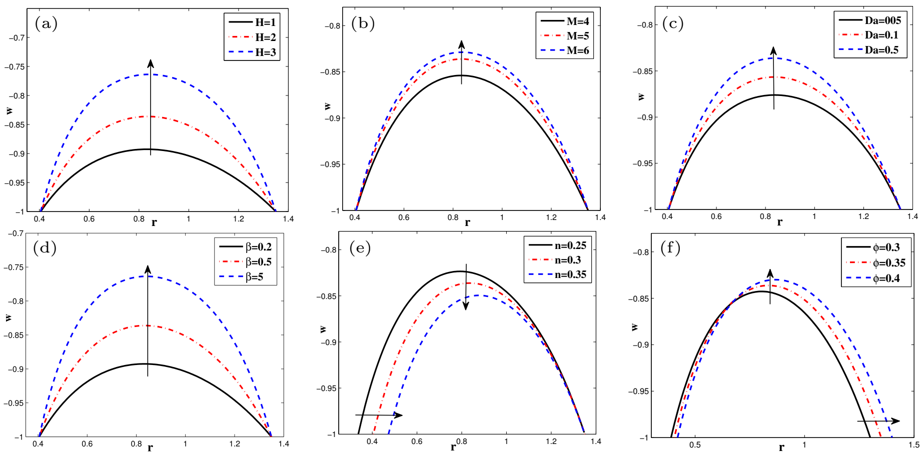

Fig. 2. Axial velocity $\frac{\partial p}{\partial z} = 2$ (a) for different values of H when $M = 5$, $\mathrm{Da} = 0.5$, $\beta = 0.5$, $n = 0.3$ and $\phi = 0.0.35$; (b) for different values of M when $H = 2$, $\mathrm{Da} = 0.5$, $\beta = 0.5$, $n = 0.3$ and $\phi = 0.5$; (c) for different values of Da when $H = 2$, $M = 5$, $\beta = 0.5$, $n = 0.3$ and $\phi = 0.35$; (d) for different values of β when $H = 2$, $M = 5$, $\mathrm{Da} = 0.5$, $n = 0.3$ and $\phi = 0.35$; (e) for different values of n when $H = 2$, $M = 5$, $\mathrm{Da} = 0.5$, $\beta = 0.5$ and $\phi = 0.5$; (f) for different values of ϕ when $H = 2$, $M = 5$, $\mathrm{Da} = 0.5$, $\beta = 0.5$ and $n = 0.3$.

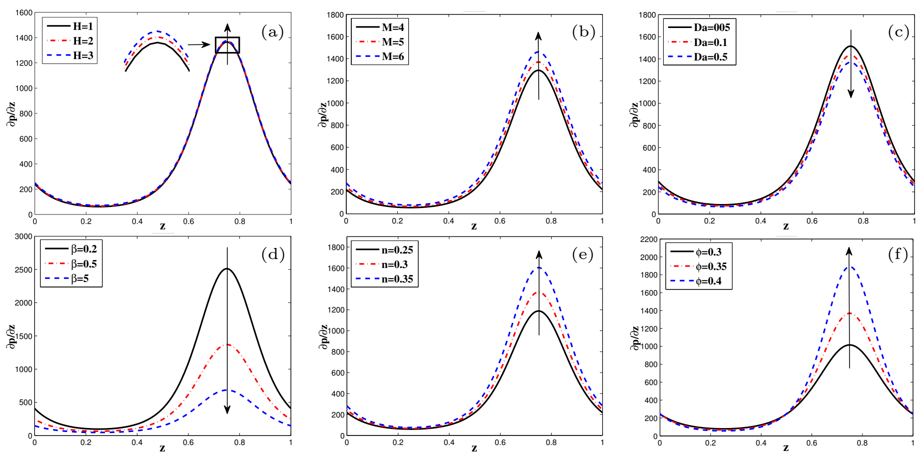

Fig. 3. Pressure gradient for $Q = -2$ (a) for different values of H when $M = 5$, $\mathrm{Da} = 0.5$, $\beta = 0.5$, $n = 0.3$ and $\phi = 0.0.35$; (b) for different values of M when $H = 2$, $\mathrm{Da} = 0.5$, $\beta = 0.5$, $n = 0.3$ and $\phi = 0.5$; (c) for different values of Da when $H = 2$, $M = 5$, $\beta = 0.5$, $n = 0.3$ and $\phi = 0.35$; (d) for different values of β when $H = 2$, $M = 5$, $\mathrm{Da} = 0.5$, $n = 0.3$ and $\phi = 0.35$; (e) for different values of n when $H = 2$, $M = 5$, $\mathrm{Da} = 0.5$, $\beta = 0.5$ and $\phi = 0.5$; (f) for different values of ϕ when $H = 2$, $M = 5$, $\mathrm{Da} = 0.5$, $\beta = 0.5$ and $n = 0.3$.

intersected in the co-pumping region ($\Delta p < 0$) *i.e.*, the pumping region, the flow rate Q_0 for zero pressure rise and the pressure rise Δp_0 for zero flow rate increase simultaneously when H and ϕ increase. Figures 4 (c)–(f) show that for different values of n, M, β and Da, the curves are intersecting in the pumping region ($\Delta p > 0$). One can see that Δp_0 increases and Q_0 decreases with increasing n and M, while the opposite behavior is observed *versus* β and Da.

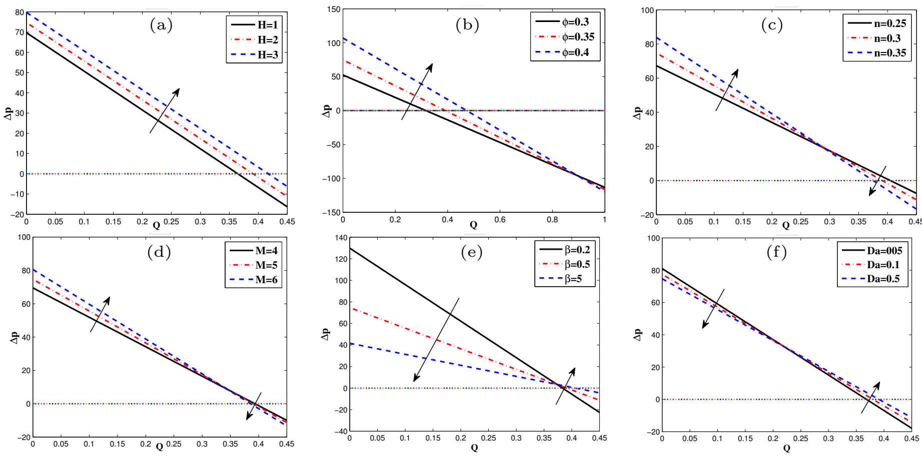

Fig. 4. Pressure rise (a) for different values of H when $M = 5$, $\mathrm{Da} = 0.5$, $\beta = 0.5$, $n = 0.3$ and $\phi = 0.0.35$; (b) for different values of ϕ when $H = 2$, $M = 5$, $\mathrm{Da} = 0.5$, $\beta = 0.5$ and $n = 0.3$; (c) for different values of n when $H = 2$, $M = 5$, $\mathrm{Da} = 0.5$, $\beta = 0.5$ and $\phi = 0.5$; (d) for different values of M when $H = 2$, $\mathrm{Da} = 0.5$, $\beta = 0.5$, $n = 0.3$ and $\phi = 0.5$; (e) for different values of β when $H = 2$, $M = 5$, $\mathrm{Da} = 0.5$, $n = 0.3$ and $\phi = 0.35$; (f) for different values of Da when $H = 2$, $M = 5$, $\beta = 0.5$, $n = 0.3$ and $\phi = 0.35$.

In order to investigate the mechanical efficiency of the pump in the peristaltic pumping region, we recall that this region is defined when the flow rate Q and the pressure rise Δp are positive. It extends from zero flow to the maximum flow rate Q_0 *i.e.*, zero pressure rise. From Eq. (20), we find the expressions of Δp_0 and Q_0 as follows:

$$\begin{aligned} \Delta p_0 &= \frac{N^3}{\alpha} I_1 + HM\,, \\ Q_0 &= -\frac{1}{I_2}\left(I_1 + \frac{\alpha MH}{N^3}\right) \end{aligned} \tag{27}$$

with

$$I_1 = \int_0^1 \frac{(1-n^2)\left(r_2^2 - 1 - \frac{\phi^2}{2}\right)}{A_6} \, \mathrm{d}z \,,$$

$$I_2 = \int_0^1 \frac{1}{A_6} \, \mathrm{d}z \,.$$

Plots in Fig. 5 illustrate Δp_0 and Q_0 over the whole possible range of the occlusion *i.e.*, $\phi = 0$ (no peristalsis) to $\phi = 1$ (complete occlusion). This figure reveals that for $\phi = 0$ and $\Delta p_0 = 0$, there is no flow $Q_0 = 0$. In addition, when $\phi \to 1$, Q_0 is maximum *i.e.*, all the fluid contained in one wavelength must be transported at speed c, whereas $\Delta p_0 \to \infty$. When $0 < Q < Q_0$, the peristaltic wave serves as a pump in the range where the mean flow is in the direction of the pressure rise. Figure 5 also shows that the flow rate Q_0 for zero pressure rise decreases with the increase in radius ratio n.

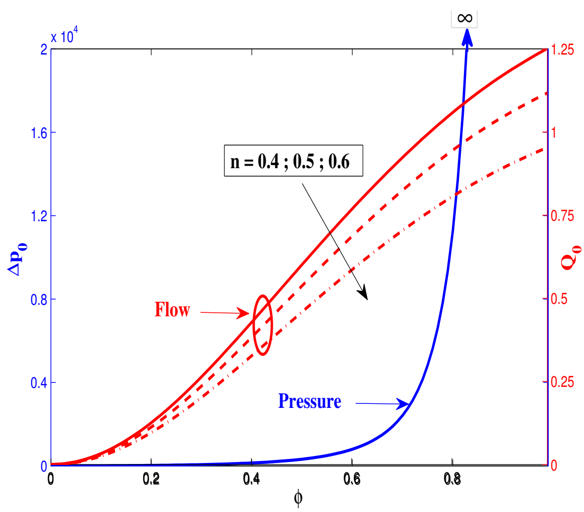

Fig. 5. Flow rate θ_0, for zero pressure rise, and pressure rise Δp_0, for zero flow rate, both as functions of amplitude ratio ϕ; effect of n on θ_0 when $H = 2$, $M = 5$, $\mathrm{Da} = 0.5$ and $\beta = 0.5$.

In Figs. 6 (a)–(f), we display the behavior of the mechanical efficiency E *versus* the ratio of time-averaged flow rate Q to Q_0 (*i.e.* $\frac{Q}{Q_0}$). It is observed that $E = 0$ for $\frac{Q}{Q_0} = 0$ (*i.e.*, no flow) and for $\frac{Q}{Q_0} = 1$ or $Q = Q_0$ (*i.e.*, no pressure rise $\Delta p = 0$). It can also be seen that the mechanical efficiency E

increases from zero to a maximum in a certain value of the ratio $\frac{Q}{Q_0}$, then it decreases to zero. In addition, the mechanical efficiency E follows the same variation of the flow rate Q in the free-pumping region ($\Delta p = 0$) *i.e.*, E increases with increasing H, ϕ, n, β and Da, while it decreases with the increase of M.

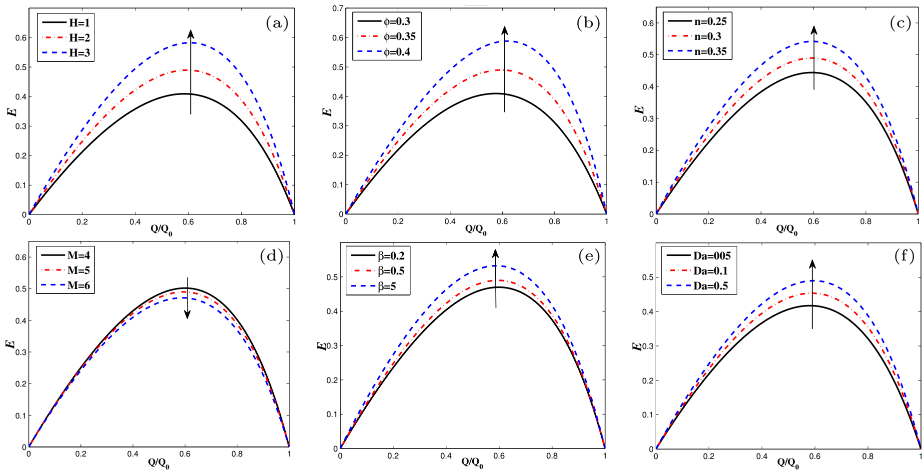

Fig. 6. Mechanical efficiency (a) for different values of H when $M = 5$, $\mathrm{Da} = 0.5$, $\beta = 0.5$, $n = 0.3$ and $\phi = 0.0.35$; (b) for different values of ϕ when $H = 2$, $M = 5$, $\mathrm{Da} = 0.5$, $\beta = 0.5$ and $n = 0.3$; (c) for different values of n when $H = 2$, $M = 5$, $\mathrm{Da} = 0.5$, $\beta = 0.5$ and $\phi = 0.5$; (d) for different values of M when $H = 2$, $\mathrm{Da} = 0.5$, $\beta = 0.5$, $n = 0.3$ and $\phi = 0.5$; (e) for different values of β when $H = 2$, $M = 5$, $\mathrm{Da} = 0.5$, $n = 0.3$ and $\phi = 0.35$; (f) for different values of Da when $H = 2$, $M = 5$, $\beta = 0.5$, $n = 0.3$ and $\phi = 0.35$.

In Figs. 7 (a)–(c), we plot the results of peristaltic flow for a biviscosity fluid compared to a Newtonian fluid in the cases of deformable, rigid and without endoscope. This comparison shows that the pressure gradient, the pumping region and the mechanical efficiency follow the same variation. These pumping characteristics are greater for a biviscosity fluid than those for a Newtonian fluid. It can also be seen that these physical quantities are smaller in the case of absence of an endoscope than in the case when an endoscope is inserted. Finally, one can observe that the deformation of endoscope walls reduces $\dfrac{\partial p}{\partial z}$ Δp and the pumping region.

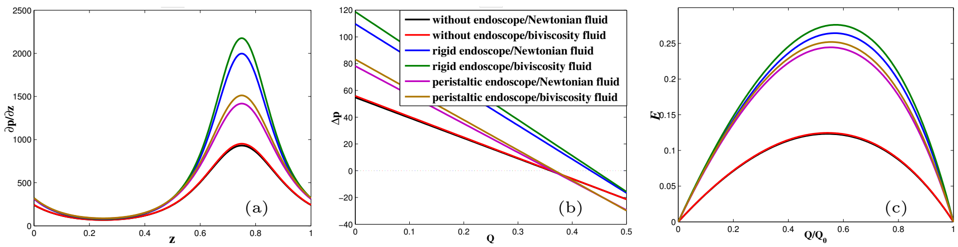

Fig. 7. Pressure gradient, pressure rise and mechanical efficiency for the Newtonian and biviscosity fluids in cases without endoscope, with rigid one or deformable one when $H = 0.5$, $M = 5$, $\beta = 5$ and $\phi = 0.4$.

4. Conclusions

The present investigation discusses the effects of electric and magnetic fields on peristaltic pumping of a biviscosity fluid between two coaxial peristaltic tubes and through porous media. The problem has been solved under long wavelength and low Reynolds number assumptions. It is observed that the electrical field strength parameter H, upper limit apparent viscosity coefficient β, Darcy number Da, occlusion ϕ and the radius ratio n enhance the pumping and the mechanical efficiency, while the Hartmann number M reduces these pumping characteristics. Moreover, the comparison with a Newtonian fluid in the cases of absence of an endoscope and in the presence of a rigid or a deformable one has been analyzed in this study.

REFERENCES

[1] T.W. Latham, M.S. Thesis, Massachusetts Institute of Technology, Cambridge 1966.

[2] M.Y. Jaffrin, A.H. Shapiro, *Annu. Rev. Fluid Mech.* **3**, 13 (1971).

[3] Y.C. Fung, C.S. Yih, *J. Appl. Mech.* **35**, 669 (1968).

[4] L.M. Srivastava, V.P. Srivastava, S.N. Sinha, *Biorheology* **20**, 153 (1983).

[5] F.M. Abbasi, T. Hayat, B. Ahmad, *Can. J. Phys.* **93**, 1190 (2015).

[6] I. Shahzadi, S. Nadeem, *Can. J. Phys.* **94**, 1319 (2016).

[7] T. Hayat, N. Ali, S. Asghar, *Acta Mech.* **193**, 101 (2007).

[8] H. Rachid, M.T. Ouazzani, *Int. J. Appl. Mech.* **6**, 1450061 (2014).

[9] N.S. Akbar, S. Nadeem, *Commun. Theor. Phys.* **56**, 761 (2011).

[10] S. Nadeem, N.S. Akbar, *Int. J. Num. Meth. Fluids.* **66**, 919 (2011).

[11] K.S. Mekheimer, *Arab. J. Sci. Eng.* **30**, 69 (2005).

[12] A.M. El Misery, Abd El Hakeem, Abd El Naby, Abd Hameed El Nagar, *J. Phys. Soc. Jap.* **72**, 89 (2003).

[13] H. Rachid, M.T. Ouazzani, M. Riahi, *Acta Phys. Pol. B* **46**, 2051 (2015).

[14] H. Rachid, M.T. Ouazzani, *Eur. Phys. J. Plus.* **130**, 122 (2015).

[15] C.H. Chen, J.G. Santiago, *J. Microelectromechanical Syst.* **11**, 672 (2002).

[16] S. Zeng, C.H. Chen, J.C. Mikkelsen Jr., J.G. Santiago, *Sens. Actuators B: Chem.* **79**, 107 (2001).

[17] K. Seibel, L. Schöler, H. Schäfer, M. Böhm, *J. Micromech. Microeng.* **18**, 025008 (2008).

[18] J. Darabi, M. Rada, Y.M. Ohadi, J. Lawler, *J. Microelectromechanical Syst.* **11**, 684 (2002).

[19] J.M. Wang, L.J. Yang, *Tamkang J. Sci. Eng.* **8**, 231 (2005).

[20] P.M. Kazemi, P.R. Selvaganapathy, C.Y. Ching, *IEEE Trans. Dielec. Elec. Insul.* **16**, 483 (2009).

[21] M. Buren, Y. Jian, L. Chang, *J. Phys. D: Appl. Phys.* **47**, 425501 (2014).

[22] D. Si, Y. Jian, *J. Phys. D: Appl. Phys.* **48**, 085501 (2015).

[23] A. Sinha, G.C. Shit, *J. Magn. Magn. Mater.* **378**, 143 (2015).

[24] I.M. Eldesoky, *Int. J. Math. Math. Sci.* **2012**, 860239 (2012).

[25] S. Hina, *J. Magn. Magn. Mater.* **404**, 148 (2016).

[26] T. Hayat, S. Hina, *Nonlinear Anal. Real World Appl.* **11**, 3155 (2010).

[27] K. Ramesh, M. Devakar, *J. Fluids* **2015**, 163832 (2015).

[28] K.S. Mekheimer, T.H. Al-Arabi, *Int. J. Math. Math. Sci.* **2003**, 1663 (2003).

[29] M. Kothandapani, S. Srinivas, *Phys. Lett. A* **372**, 4586 (2008).

[30] J.C. Misra, S. Maiti, G.C. Shit, *J. Mech. Med. Biol.* **8**, 507 (2008).

[31] M. Nakamura, T. Sawada, *J. Non-Newt. Fluid Mech.* **22**, 191 (1987).

[32] M. Nakamura, T. Sawada, *J. Biomech. Eng.* **110**, 137 (1988).

[33] A.H. Shapiro, M.Y. Jaffrin, S.L. Weinberg, *J. Fluid Mech.* **37**, 799 (1969).

[34] H. Rachid, M.T. Ouazzani, *Int. J. Appl. Mechanics* **8**, 1650056 (2016).